Knockdown of CCT2 inhibits the malignant progression of hepatocellular carcinoma cells by impairing STAT3 activation

CHAO LI[1], LEI YANG[2], YUDONG ZHANG[1], BAOCHENG ZHAO[1] and HAO QU[1]

[1]Division of Gastrointestinal Surgery, Department of General Surgery, Beijing Chao-Yang Hospital, Capital Medical University, Beijing 100020, P.R. China; [2]Medical Research Center, Beijing Chao-Yang Hospital, Capital Medical University, Beijing 100020, P.R. China

Received October 24, 2025; Accepted January 30, 2026

DOI: 10.3892/or.2026.9086

Abstract. Hepatocellular carcinoma (HCC) is an aggressive liver malignancy, the molecular mechanisms underlying the progression of which are not fully understood. As a component of the chaperonin-containing tailless complex polypeptide 1 (TCP1) ring complex, chaperonin-containing TCP1 subunit 2 (CCT2) participates in the development of numerous types of liver disease. However, the potential role of CCT2 in regulating HCC malignant behaviors remains unclear. In the present study, bioinformatics analysis of patients with HCC from public datasets (The Cancer Genome Atlas-Liver HCC, International Cancer Genome Consortium-Liver Cancer-Riken-Japan and OEP00000321) demonstrated that CCT2 expression was upregulated in HCC tissue. High expression of CCT2 was also associated with an unfavorable overall survival prognosis. CCT2 knockdown was shown to inhibit the proliferation, migration, invasion and stemness and promote the apoptosis of HCC cells *in vitro*, as evidenced by EdU, colony formation, flow cytometry, caspase-3/7 activity, gap closure, Transwell and tumor-sphere formation assays. Consistently, knocking down CCT2 also suppressed the subcutaneous tumor proliferation and hematogenous lung metastasis of the human HCC HCCLM3 cells *in vivo*. Furthermore, downregulation of CCT2 decreased the phosphorylation of STAT3, as well as the expression of myeloid cell leukemia sequence 1, matrix metalloproteinase 2 and SRY-box transcription factor 2 *in vitro* and *in vivo*. However, IL-6 treatment rescued the levels of phosphorylated STAT3 and counteracted the inhibitory effects of CCT2 knockdown on proliferation and invasion. The findings suggest that CCT2 promotes HCC by activating the STAT3 signaling pathway. Therefore, CCT2 may serve as a survival biomarker and precision treatment target in HCC.

Correspondence to: Professor Hao Qu, Division of Gastrointestinal Surgery, Department of General Surgery, Beijing Chao-Yang Hospital, Capital Medical University, 8 Gongti South Road, Chaoyang, Beijing 100020, P.R. China
E-mail: 13701320206@163.com

Key words: chaperonin-containing tailless complex polypeptide subunit 2, hepatocellular carcinoma, proliferation, invasion, stemness, signal transducer and activator of transcription 3

Introduction

Based on epidemiological data in 2020, primary liver cancer is the third leading cause of cancer-associated death globally, accounting for ~830,2000 deaths. Hepatocellular carcinoma (HCC) accounts for 90% of the primary liver cancer incidence (1,2). Over the past two decades, molecular targeted agents have emerged as promising therapeutic options for HCC (3). However, the prognosis of patients with HCC remains unfavorable due to the aggressive growth and metastasis of this cancer. Therefore, a deeper understanding of HCC pathogenesis remains essential.

Chaperonins are a cluster of molecular chaperones with sizes ranging from 55 to 64 kDa (4) that are divided into groups I and II according to their distinct encapsulation mechanism. The tailless complex polypeptide 1 (TCP1) ring complex belongs to group II and comprises eight distinct subunits (5). The classical functions of the TCP1 ring complex include a chaperone that is key for the correct folding of polypeptide substrates and an autophagy receptor involved in regulating the degradation of solid protein aggregates (6,7). Numerous chaperonin-containing TCP1 (CCT) subunits have been shown to regulate HCC progression; specifically, knockdown of CCT3 sensitizes HCC cells to sorafenib and enhances sorafenib-mediated ferroptosis (8). Inhibiting CCT4 induces securin and Bim accumulation, which causes HCC cell apoptosis (9). Depletion of CCT8 arrests the cell cycle in the G0/G1 phase by inhibiting CDK2 and cyclin E expression in Huh-7 cells (10). *In silico* analysis has indicated that CCT2 expression is markedly upregulated in breast and pancreatic cancer and thyroid carcinoma (11). The clinical value and biological functions of CCT2 in HCC progression remain poorly understood, however, CCT2 has been observed to promote tumor viability, stemness and metastasis in breast and lung cancer (12,13).

STAT3 is the most well-known member of the STAT family (14). Phosphorylation of STAT3 at the Tyr705 and Ser727 residues are prerequisites of STAT3 signaling activation (15). Although over-activation of STAT3 is noted in numerous types of liver disease, including viral hepatitis (16), hepatic ischemia-reperfusion injury (17) and liver fibrosis (18), its role in HCC is notable as the STAT3 signaling pathway

regulates the proliferation, stemness and metastasis of HCC cells (19). However, the regulatory effects of CCT2 in STAT3 activation remain ambiguous. Chen *et al* (20) reported that over-activation of STAT3 signaling is crucial for the CCT2-mediated proliferation and invasion of triple-negative breast cancer cells. By contrast, Vallin *et al* (21) found that the levels of STAT3 phosphorylation at Tyr705 increase following CCT2 knockout in the estrogen receptor positive and progesterone receptor positive MCF-7 breast cancer cell line. Genetic heterogeneity between cell lines may be how CCT2 achieves different roles in the STAT3 signaling pathway. The association between CCT2 expression and STAT3 signaling activation in HCC remains unclear.

The present study systematically investigated the effects of CCT2 knockdown on the malignant properties and STAT3 signaling activation in HCC cells. The findings of the present study may facilitate the translational application of CCT2 in HCC molecular targeted therapy in the future.

Materials and methods

Public dataset acquisition. The Cancer Genome Atlas-Liver HCC (TCGA-LIHC) (22), International Cancer Genome Consortium-Liver Cancer-Riken, Japan (ICGC-LIRI-JP) (23) and OEP00000321 (24) preprocessed datasets were downloaded from the HCC database (lifeome.net:809/#/download) (25). Based on the median expression of CCT2 calculated in HCC tissue (11.17 in TCGA-LIHC, 5.40 in ICGC-LIRI-JP and 11.41 in NODE-OEP00000321), patients were stratified into high and low CCT2 expression groups. The association between CCT2 expression and overall survival was assessed by Kaplan-Meier analysis using GraphPad Prism 10 software (Dotmatics).

Cell culture. The HCC cell lines Huh-7 (cat. no. STCC10102G), Hep3B (cat. no. STCC10103G), Li-7 (cat. no. STCC10107G) and HCCLM3 (cat. no. STCC10111G) were provided by Wuhan Servicebio Technology Co., Ltd. STR profiling was performed to ensure the authenticity of cells. Complete culture medium was prepared with DMEM (cat. no. C11995500BT) supplemented with 10% FBS (cat. no. A5256701; both Gibco; Thermo Fisher Scientific, Inc.) and 1% penicillin-streptomycin solution (cat. no. P4333; Sigma-Aldrich; Merck KGaA). The cells were incubated in complete culture medium at 37˚C under a humidified environment with 5% CO_2. Recombinant human IL-6 (cat. no. HY-P7044; MedChemExpress) as used for STAT3 activation. In brief, Huh-7 and HCCLM3 cells were treated with IL-6 (50 ng/ml) or PBS at 37˚C for 24 h and cells were collected for further experiments.

Lentivirus transduction. Huh-7 and HCCLM3 cells were seeded into 6-well plates at a density of $1x10^5$ cells/well and incubated at 37˚C overnight. As previously described (26), shRNA plasmids and packaging plasmids were co-transfected into 293T cells at 37˚C for 8 h. Mature lentiviral particles ($1x10^8$ TU/ml) carrying CCT2-specific short hairpin (sh)RNA (sh-CCT2) or negative control shRNA (sh-NC) were provided by Shanghai GeneChem Co., Ltd. The sequence for human CCT2 shRNA was 5'-TTCATCCACAGACCATCATAG-3'. The sequence for human sh-NC was 5'-TTCTCCGAACGTGTCACGT-3'. The lentiviral transduction of HCC cells was performed at a multiplicity of infection of 10. Following 12 h transduction at 37˚C, the viral medium was replaced with fresh complete medium. To select stably transduced cells, puromycin was applied at a concentration of 5 μg/ml for 48 h. The viable cells were maintained in culture medium containing 1.25 μg/ml puromycin for continuous passaging. Expression of CCT2 was detected by reverse transcription-quantitative PCR (RT-q)PCR and western blot analysis. Subsequent experiments were performed ≥72 h after lentiviral transduction.

EdU incorporation assay. Huh-7 and HCCLM3 cells were cultured in 6-well plates at an initial seeding density of $1x10^5$ cells/well. Following a 3 h light-protected incubation at 37˚C with 0.1% EdU reagent (cat. no. C10310-1; Guangzhou RiboBio Co., Ltd.), the cells were fixed using 4% paraformaldehyde (PFA) for 30 min at room temperature. The incorporated EdU was detected by treating the cells with Apollo staining reagent (cat. no. C10371-1; Guangzhou RiboBio Co., Ltd.) for 30 min at room temperature. The cell nuclei were stained with Hoechst 33342 reagent for 30 min at room temperature. Fluorescence images were captured using the Operetta CLS high-content analysis system (PerkinElmer, Inc.). In total, five visual fields were chosen at random and the number of EdU positive cells was evaluated using ImageJ software (version 1.53 K; National Institutes of Health). The proportion of EdU-positive cells was calculated as follows: (EdU-positive cells/total cells) x100%.

Colony formation assay. Huh-7 and HCCLM3 cells were cultured in 6-well plates at an initial seeding density of $1x10^3$ cells/well. The complete DMEM in the wells was refreshed at 3 day intervals. Following 14 day culture, 4% PFA and 0.1% crystal violet were added to the plates for fixation (30 min at room temperature) and staining (20 min at room temperature), respectively. The cell colonies consisting of ≥40 cells were observed using the ECLIPSE Ts2 inverted light microscope (Nikon Corporation) and counted using ImageJ software.

Flow cytometry. Early and late apoptotic cells were labeled using Annexin V-PE/7-AAD (cat. no. KGA1104; Nanjing KeyGen Biotech Co., Ltd.). Huh-7 and HCCLM3 cells were digested with EDTA-free trypsin. Then, $1x10^5$ cells were resuspended in 500 μl binding buffer working solution to prepare a single-cell suspension. For each 500 μl cell suspension, 1 μl Annexin V-PE and 5 μl 7-AAD were sequentially added. After mixing by vortexing, the tubes were kept in the dark for 10 min to ensure complete reactions. The FACSAria II flow cytometer (BD Biosciences) was used to measure the percentage of apoptotic cells. Cell apoptosis was analyzed by FACSDiva Software (v6.1.3, BD Biosciences).

Apo-ONE homogeneous caspase-3/7 assay. Huh-7 or HCCLM3 cells were resuspended in DMEM at a density of $1x10^5$ cells/ml. Then, 100 μl Apo-ONE caspase-3/7 substrate working solution (cat. no. G7792; Promega Corporation) and 100 μl cell suspension were sequentially added to a black 96-well cell culture plate. The contents were mixed using a plate shaker. The cells were incubated at room temperature,

protected from the light, for 8 h. The fluorescence of each well was measured using the FL 6500 spectrofluorometer (PerkinElmer, Inc.), as previously described (27).

Gap closure assay. Ibidi Culture-Insert 25 Well plates (cat. no. 80209; ibidi GmbH) were used for the gap closure assay. $3x10^5$ Huh-7 or HCCLM3 cells were cultured in the wells until they formed 100% confluent monolayers, at which point the inserts were removed. The cells were cultured in serum-free DMEM (Thermo Fisher Scientific, Inc.) at 37˚C for an additional 48 h. In total, five independent repeats were performed for each group. Images were captured by the ECLIPSE Ts2 inverted light microscope at 0 and 48 h. The gap area was measured by ImageJ software and calculated as follows: Gap closure ratio (%)=[1-(area at 48 h/area at 0 h)] x100%.

Transwell assay. DMEM-Matrigel (10%; cat. no. 354234; Corning, Inc.) was used to precoat the upper surface of permeable Transwell insert membranes (cat. no. 3464; Corning, Inc.) for 2 h at 37˚C. The inserts were placed in a 24-well plate. Next, $2x10^4$ Huh-7 or HCCLM3 cells were resuspended in 200 μl serum-free DMEM and added to the upper chamber of the Transwell insert, while the lower chamber was filled with 600 μl complete DMEM. Following a 24 h culture at 37˚C, the inserts were incubated with 4% PFA and 0.1% crystal violet for fixation (30 min at room temperature) and staining (20 min at room temperature), respectively. The successfully invaded cells were counted under the ECLIPSE Ts2 inverted light microscope.

Tumor sphere formation assay. Suspended single Huh-7 or HCCLM3 cells ($1x10^3$) were cultured with Tumor Stem Cell Pellet Culture Medium (serum-free; cat. no. P2401; Shanghai QiDa Biotechnology Co., Ltd) in ultra-low attachment plates (24-well; cat. no. 3473; Corning, Inc.). Following 14 days incubation at 37˚C, cell spheres were counted under the ECLIPSE Ts2 inverted light microscope. The spheroid formation efficiency (SFE) was calculated as follows: SFE (%)=number of spheres/1,000x100%. Furthermore, tumor spheres were harvested and digested into a single-cell suspension for EdU incorporation assay and Transwell assay.

RT-qPCR. Total RNA from Huh-7 and HCCLM3 cells was extracted using TRIzol™ reagent (Invitrogen; Thermo Fisher Scientific, Inc.) according to the manufacturer's instructions. RT-qPCR was performed using the SuperScript™ III Platinum™ One-Step qRT-PCR kit (cat. no. 11732020; Invitrogen; Thermo Fisher Scientific, Inc.). The one-step thermocycling conditions were as follows: 50˚C for 15 min to synthesize cDNA; 95˚C for 2 min to denaturalize the cDNA and activate the Taq DNA Polymerase; 40 cycles of 95˚C for 15 sec (denaturation) and 60˚C for 30 sec (annealing and extension). The $2^{-\Delta\Delta Cq}$ method was used to calculate the relative expression of the target genes (28,29). The primers were as follows: CCT2 forward, 5'-GCACTACCTCTGTTACCGTTTT-3' and reverse, 5'-CTTCTCTCCAACCCGCTATGA-3' and β-actin (reference gene) forward, 5'-CATGTACGTTGCTATCCAGGC-3' and reverse, 5'-CTCCTTAATGTCACGCACGAT-3'.

Western blotting. RIPA buffer (cat. no. P0013B) and the BCA Protein Assay kit (cat. no. P0012; both Beyotime Institute of Biotechnology) were used to extract the total protein from Huh-7 and HCCLM3 cells and measure the protein concentration, respectively. The same mass of protein (40 μg/lane) was separated by 4-20% SDS-PAGE (cat. no. P0468S; Beyotime Institute of Biotechnology) and then transferred onto PVDF membranes (cat. no. IPVH00010; MilliporeSigma). The membranes were washed with TBS for 10 min at room temperature. The membranes were blocked with 5% fat-free milk for 1 h at room temperature followed by incubation with primary antibodies (1:1,000 using 5% fat-free milk) at 4˚C overnight. The primary antibodies were as follows: CCT2 (cat. no. 24896-1-AP), β-actin (cat. no. 66009-1-Ig), MMP2 (cat. no. 10373-2-AP), myeloid cell leukemia sequence 1 (MCL1; cat. no. 16225-1-AP) and SRY-box transcription factor 2 (SOX2; cat. no. 11064-1-AP; all Proteintech Group, Inc.) and STAT3 (cat. no. 4904) and phosphorylated (p-)STAT3 (Tyr705; cat. no. 4113; both Cell Signaling Technology, Inc.) The membranes were washed three times in TBST (0.1% Tween-20) for 5 min each at room temperature. The proteins were labeled with HRP-conjugated secondary antibodies (1:5,000 in 5% fat-free milk; cat. nos. SA00001-1 and SA00001-2; Proteintech Group, Inc.) for 1 h at room temperature. The membranes were washed three times in TBST for 5 min each at room temperature. Chemiluminescent signals were detected by an enhanced chemiluminescence kit (cat. no. WBKLS0500; MilliporeSigma). The band densitometry was quantified by ImageJ software.

Subcutaneous xenograft and hematogenous lung metastasis model. A total of 20 BALB/c (age, 4-6 weeks; weight, 16-18 g) male nude mice were acquired from SPF Biotechnology Co. Ltd. and raised in a specialized pathogen-free environment (25˚C, 45% humidity, 12/12-h light/dark period and *ad libitum* access to diet and water). The institutional animal care and use committee of SPF Biotechnology Co., Ltd (Beijing, China). approved the animal experiment protocol (approval no. AWE2023102504). Nude mice were randomly assigned into four groups (sh-NC and sh-CCT2 for the xenograft and hematogenous lung metastasis model; n=5/group) using random number table method. For the xenograft model, a 150 μl single-cell suspension containing $2x10^6$ transduced HCCLM3 cells (with sh-NC or sh-CCT2) was administered via subcutaneous injection into the left forelimb. Once the subcutaneous tumors were palpable, they were monitored three times per week. Tumor diameters were measured using a vernier caliper. Tumor volumes were determined as follows: Volume (mm^3)=a x b^2x0.5, where a indicates the length and b indicates the width. The tumor volume did not exceed 2,000 mm^3, in compliance with animal ethics requirements. For the lung metastasis model, a single cell suspension of $1x10^5$ transduced HCCLM3 cells (with sh-NC or sh-CCT2) in 100 μl sterile saline was administered into mice via tail vein injection. After 28 days, all animals were placed in a chamber ventilated with CO_2 at 30-70% of its volume/min. The mice were left in the chamber for ≥5 min after respiratory arrest and observed to ensure the cessation of breathing and heartbeat. Cervical dislocation (with the confirmation of a gap between the skull and spinal column) was used to ensure the death. For the xenograft model, subcutaneous tumors were dissected and weighed.

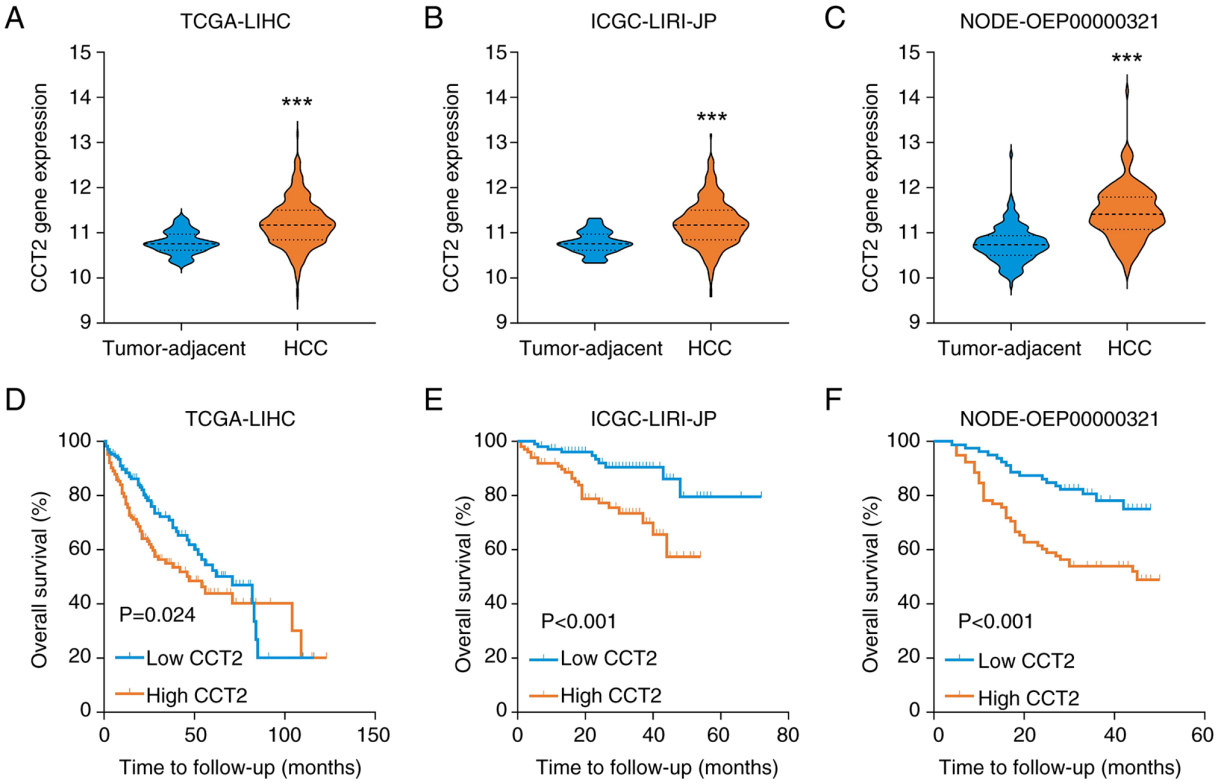

Figure 1. *In silico* analysis of CCT2 expression and the clinical significance in HCC. Transcription levels of CCT2 in (A) TCGA-LIHC, (B) ICGC-LIRI-JP and (C) NODE-OEP00000321 datasets. ***P<0.001 vs. tumor-adjacent. Association between CCT2 expression and the overall survival prognosis of patients in (D) TCGA-LIHC, (E) ICGC-LIRI-JP and (F) NODE-OEP00000321 datasets. CCT2, chaperonin containing TCP1 subunit 2; TCGA-LIHC, The Cancer Genome Atlas-liver hepatocellular carcinoma; ICGC-LIRI-JP, International Cancer Genome Consortium-liver Cancer-Riken, Japan; NODE, National Omics Data Encyclopedia; HCC, hepatocellular carcinoma.

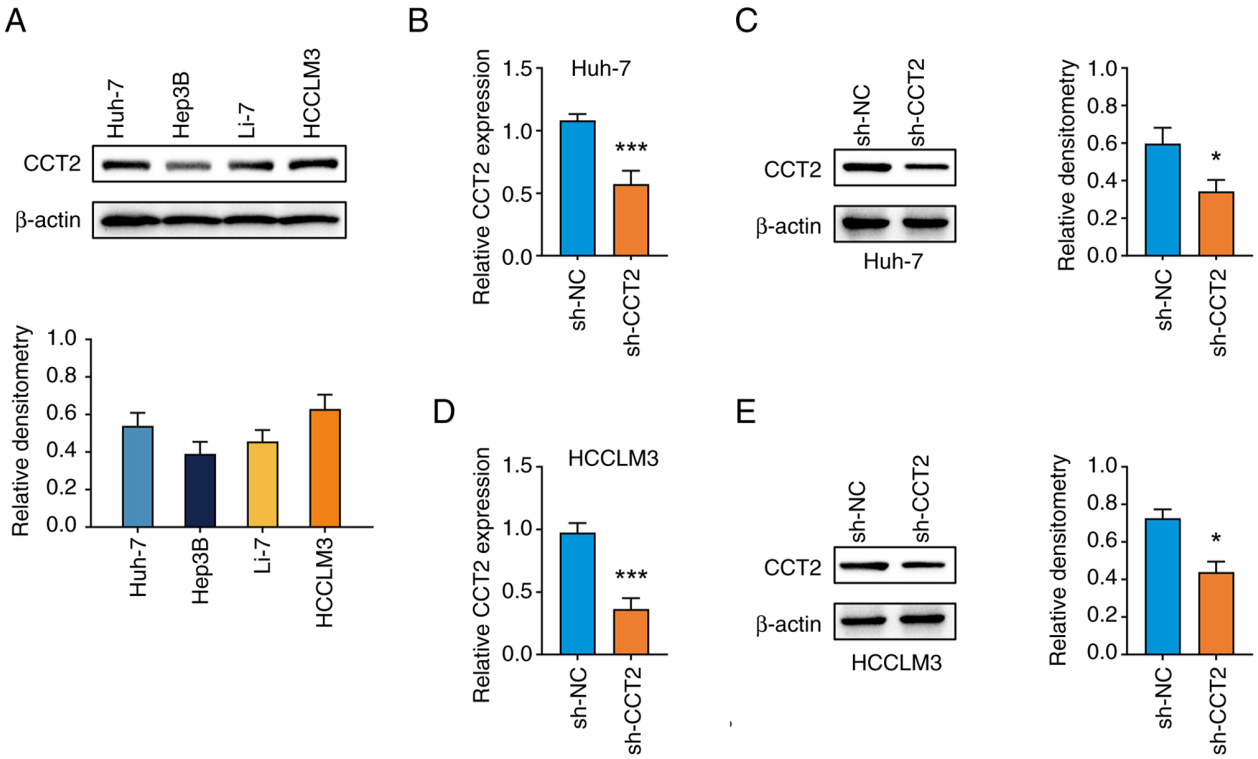

Figure 2. Knockdown of CCT2 in HCC cells. (A) Protein expression levels of CCT2 in HCC cell lines (Huh-7, Hep3B, Li-7 and HCCLM3). CCT2 was successfully knocked down in both Huh-7 and HCCLM3 cells following sh-CCT2 transduction. Knockdown efficiency in Huh-7 cells was evaluated by (B) reverse transcription-quantitative PCR and (C) western blotting. Knockdown efficiency in HCCLM3 cells was evaluated by (D) reverse transcription-quantitative PCR and (E) western blotting. *P<0.05, ***P<0.001 vs. sh-NC. CCT2, chaperonin containing TCP1 subunit 2; sh, short hairpin; NC, negative control; HCC, hepatocellular carcinoma.

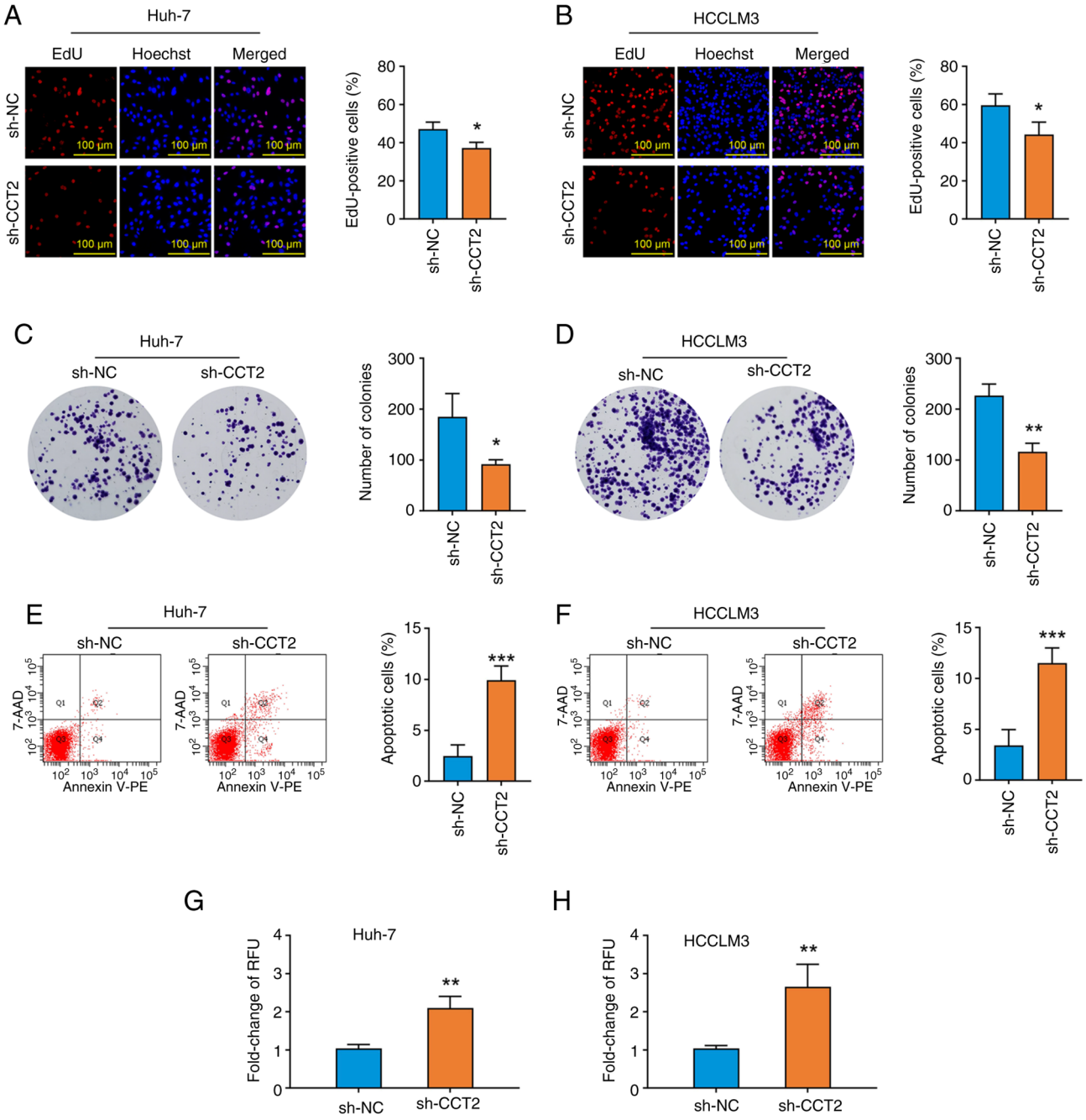

Figure 3. Knockdown of CCT2 inhibits the proliferation and promotes the apoptosis of hepatocellular carcinoma cells. EdU incorporation assay was used to determine the DNA replication activity of (A) Huh-7 and (B) HCCLM3 cells. Colony formation assay was used to assess the cell clonogenicity of (C) Huh-7 and (D) HCCLM3 cells. Flow cytometry assay was used to analyze the percentage of apoptotic (E) Huh-7 and (F) HCCLM3 cells. Caspase-3/7 activity assay was used to evaluate the degree of apoptosis in (G) Huh-7 and (H) HCCLM3 cells. *P<0.05, **P<0.01, ***P<0.001 vs. sh-NC. CCT2, chaperonin containing TCP1 subunit 2; sh, short hairpin; NC, negative control; RFU, relative fluorescence units.

For the lung metastasis model, both lungs were dissected. The tumor and lung were fixed with 4% PFA for 30 min at room temperature for further experiments.

Immunohistochemistry and hematoxylin and eosin (H&E) staining. PFA-fixed subcutaneous tumor and lung tissue were first embedded in paraffin and then sliced into 4-μm-thick sections. The sections were dewaxed in xylene (three times for 10 min each) and rehydrated through graded ethanol (100, 95, 90, 80 and 70%, 5 min each). For immunohistochemistry, antigen retrieval was performed by microwaving at 95˚C for 10 min with Tris-EDTA buffer (pH 9.0; cat. no. PR30002; Proteintech Group, Inc.). Endogenous peroxidase activity quenching and non-specific antigen blocking were performed using IHC Detect kit for Rabbit/Mouse Primary Antibody (cat. no. PK10006; Proteintech Group, Inc.). The primary antibodies, including p-STAT3 (cat. no. 4113, Cell Signaling Technology), MCL1 (cat. no. 16225-1-AP), MMP2 (cat. no. 10373-2-AP) and SOX2 (cat. no. 11064-1-AP; all Proteintech Group, Inc.), were diluted 1:100 in antibody diluent (cat. no. PR30016; Proteintech Group, Inc.) and applied at 4˚C overnight. Afterward, the sections were washed with PBS to eliminate any unbound primary antibodies and

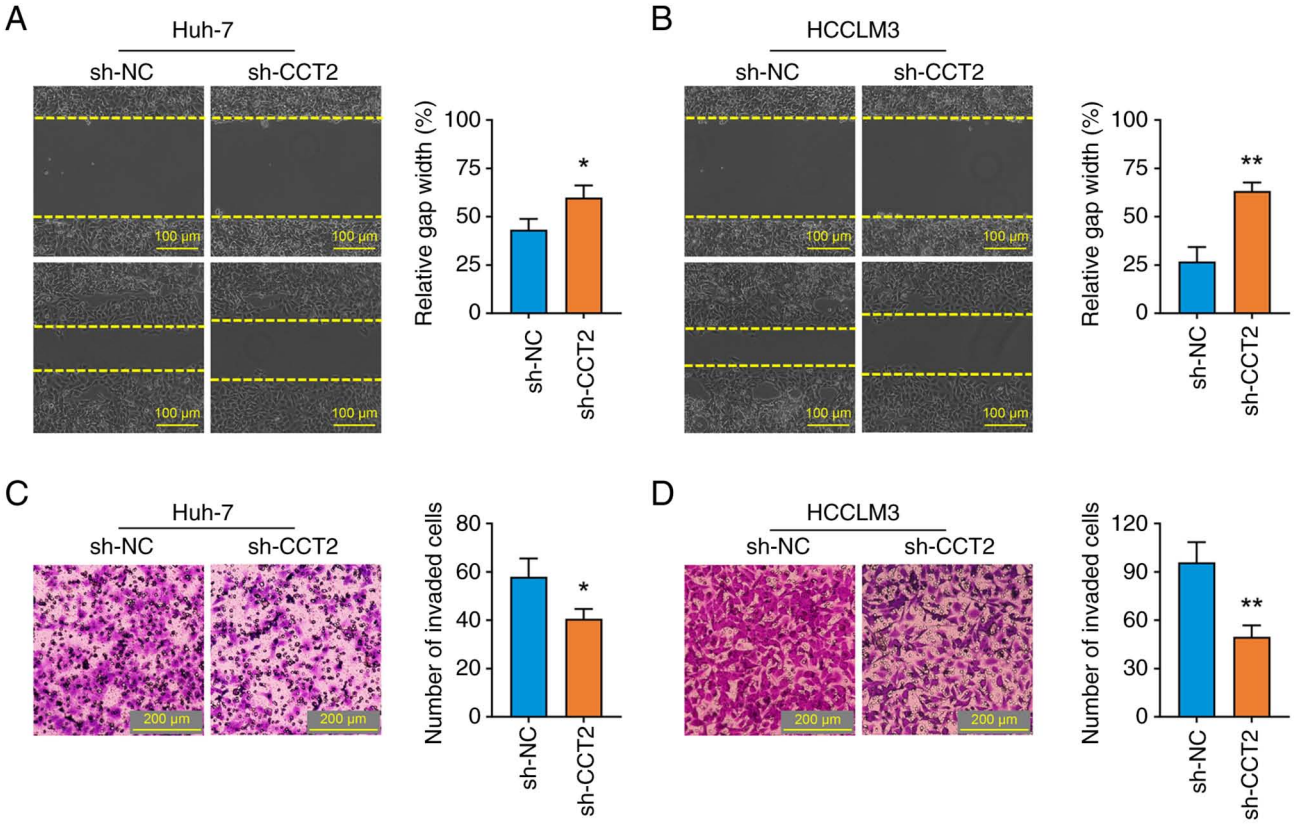

Figure 4. Knockdown of CCT2 inhibits the migration and invasion of hepatocellular carcinoma cells. The effect of CCT2 knockdown on the migration of (A) Huh-7 and (B) HCCLM3 cells was measured using gap closure assay. The effects of CCT2 knockdown on the invasion of (C) Huh-7 and (D) HCCLM3 cells was evaluated by Transwell assay. *P<0.05, **P<0.01 vs. sh-NC. CCT2, chaperonin containing TCP1 subunit 2; sh, short hairpin; NC, negative control.

subsequently incubated with 100 μl ready-to-use HRP-conjugated polymer secondary antibodies (cat. no. RGAU011, Proteintech Group, Inc.) for 30 min at room temperature. DAB was used to visualize proteins. Hematoxylin reagent was utilized to stain the nuclei for 1 min at room temperature.

For H&E staining, the sections were dipped in hematoxylin reagent for 5 min at room temperature followed by washing in flowing tap water. Then, the sections were immersed in acid alcohol (1% hydrochloric acid in 70% alcohol) for 5 sec and washed in flowing tap water until they turned blue. Eosin solution (1%) was used to stain the sections for 20 sec at room temperature.

All sections were imaged using the ECLIPSE Ts2 inverted light microscope. The mean optical density was calculated by ImageJ software to assess the expression of the target protein in the subcutaneous tumor tissues. The number of lung nodules was counted to evaluate the tumor metastatic capacity.

Statistical analysis. Quantitative data are reported as the mean ± standard deviation of ≥3 independent experimental repeats. The unpaired Student's t-test was performed to evaluate differences between two groups when data passed Shapiro-Wilk normality and equal variance test; otherwise, the Mann-Whitney test was used. The differences between >2 groups were compared by one-way ANOVA, with Tukey's post hoc test. GraphPad Prism 10 software (Dotmatics) was used for data analysis. P<0.05 was considered to indicate a statistically significant difference.

Results

Upregulated CCT2 expression is associated with poor prognosis in HCC. To evaluate the clinical significance of CCT2 in HCC, the association between CCT2 expression and OS was analyzed using multiple public HCC datasets. The results across all datasets demonstrated CCT2 expression was upregulated in HCC tissues compared with tumor-adjacent tissue (Fig. 1A-C). Kaplan-Meier curve analyses demonstrated that patients with HCC with high levels of CCT2 had a poorer OS prognosis. The hazard ratios (HRs) for OS were as follows: HR=1.51 [95% confidence interval (CI), 1.06-2.16; P=0.024; Fig. 1D] in TCGA-LIHC cohort, HR=3.12 (95% CI, 1.59-6.11; P<0.001; Fig. 1E) in the ICGC-LIRI-JP cohort and HR=2.59 (95% CI, 1.51-4.43; P<0.001; Fig. 1F) in the NODE-OEP00000321 cohort. Taken together, high expression of CCT2 may be considered a risk factor for patients with HCC.

CCT2 expression is inhibited in Huh-7 and HCCLM3 cells by lentivirus transduction. To elucidate the biological functions of CCT2 in HCC malignancy, the expression of CCT2 in HCC cell lines was detected by western blotting (Fig. 2A). Huh-7 and HCCLM3 cell lines were selected for subsequent experiments due to their relatively high levels of CCT2 expression. CCT2 expression was knocked down in Huh-7 and HCCLM3 cells by lentivirus-mediated sh-CCT2 transduction. RT-qPCR and western blotting confirmed that, compared with the sh-NC group, the mRNA (Fig. 2B and D) and protein (Fig. 2C and E)

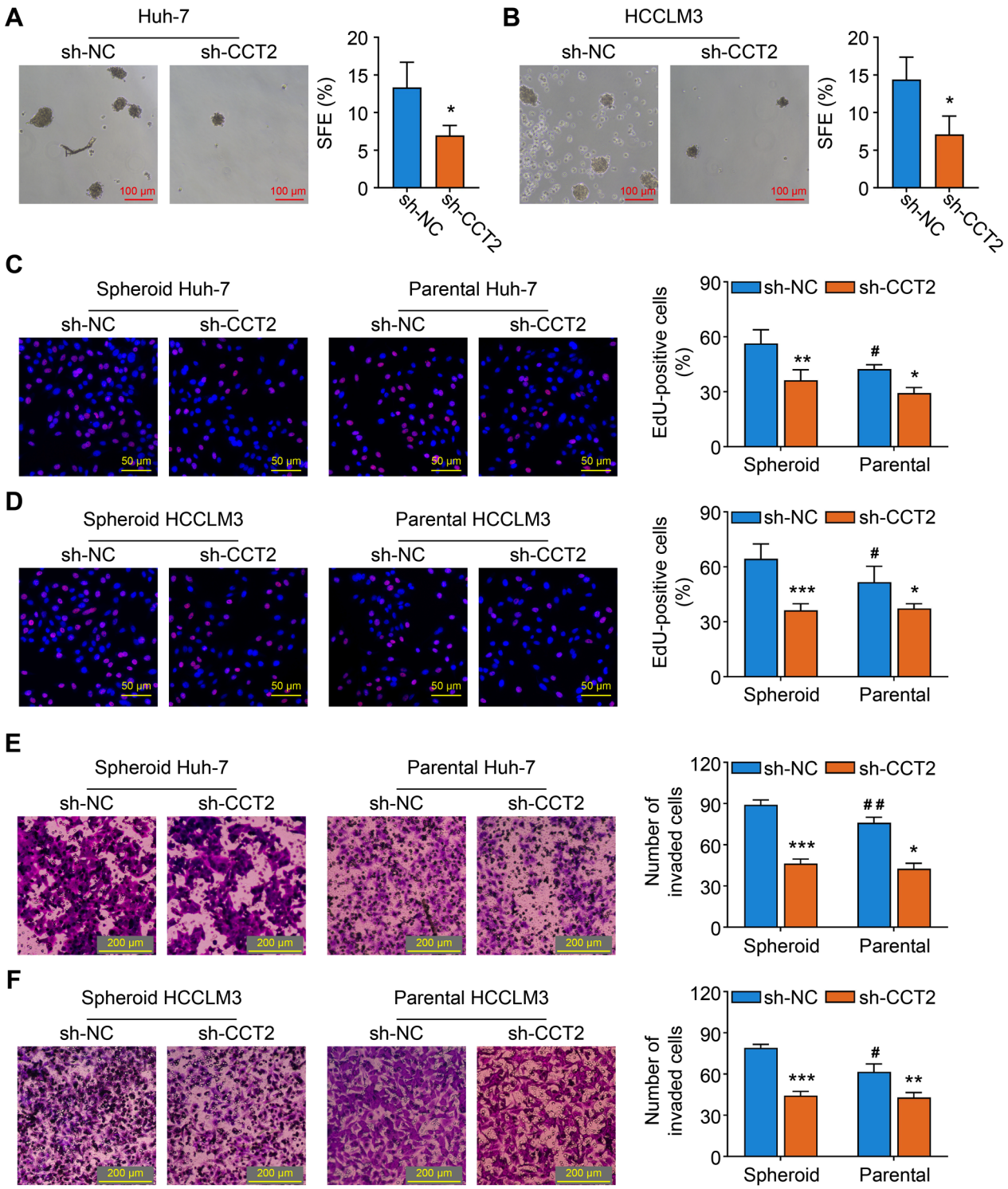

Figure 5. Knockdown of CCT2 inhibits the stemness characteristics of hepatocellular carcinoma cells. Tumor-sphere formation assay was used to assess the stem cell-like properties of (A) Huh-7 and (B) HCCLM3 cells following CCT2 knockdown. EdU incorporation assay was used to determine the proliferation of spheroid and parental (C) Huh-7 and (D) HCCLM3 cells following CCT2 knockdown. Transwell assay were used to evaluate the invasion of spheroid and parental (E) Huh-7 and (F) HCCLM3 cells following CCT2 knockdown. *P<0.05, **P<0.01, ***P<0.001 vs. parental sh-NC; $^{\#}$P<0.05, $^{\#\#}$P<0.01 vs. spheroid sh-NC. CCT2, chaperonin containing TCP1 subunit 2; sh, short hairpin; NC, negative control. SFE, spheroid formation efficiency.

levels of CCT2 were significantly downregulated in the sh-CCT2 group.

Knockdown of CCT2 inhibits proliferation and promotes the apoptosis of HCC cells. Functional experiments were performed to determine whether CCT2 knockdown affected HCC cell viability. CCT2 knockdown significantly decreased the percentage of EdU-positive cells (Fig. 3A and B) and the number of colonies formed (Fig. 3C and D). Additionally, compared with the sh-NC group, the proportion of apoptotic cells (Fig. 3E and F) and the activity of caspase-3/7 (Fig. 3G and H) increased in the CCT2 knockdown group.

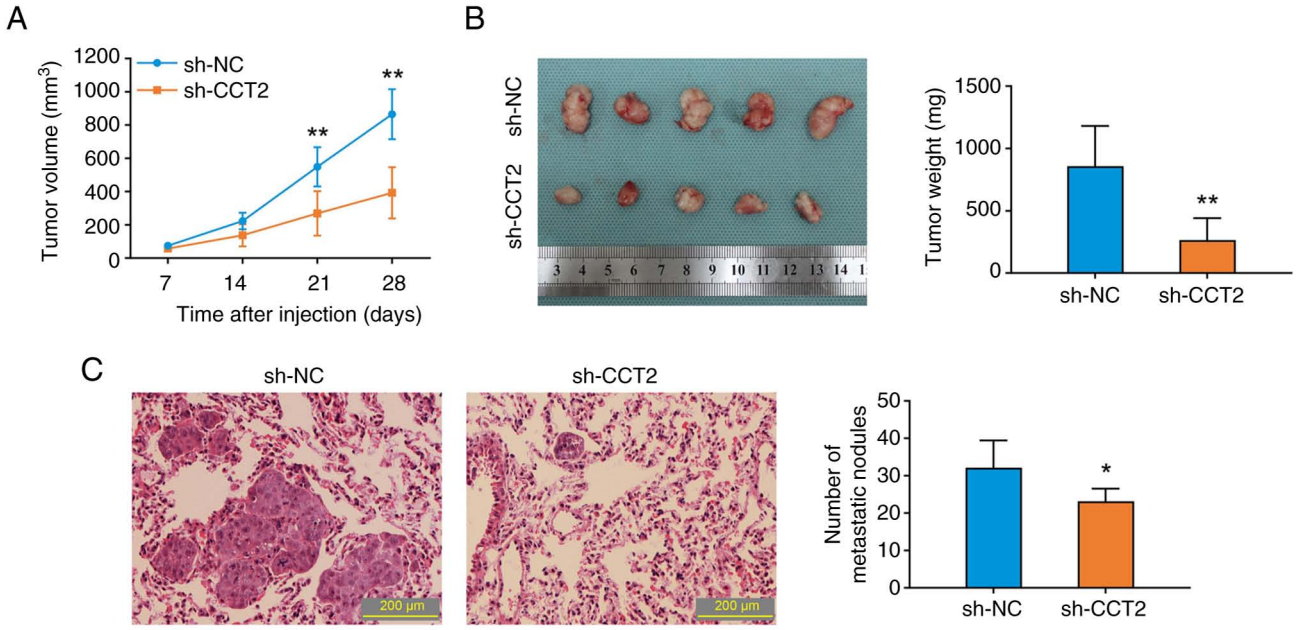

Figure 6. Knockdown of CCT2 inhibits the tumor proliferation and metastasis of HCCLM3 cells *in vivo*. Tumor (A) proliferation and (B) weights were measured to assess the effects of CCT2 knockdown on HCCLM3 tumor proliferation in nude mice. (C) Number of metastatic nodules stained with hematoxylin and eosin was calculated to evaluate the effects of CCT2 knockdown on the hematogenous lung metastasis of HCCLM3 cells (n=5/group). *P<0.05, **P<0.01 vs. sh-NC. CCT2, chaperonin containing TCP1 subunit 2; sh, short hairpin; NC, negative control.

Collectively, the findings indicated that CCT2 may be involved in the regulation of cell proliferation and apoptosis in HCC.

Knockdown of CCT2 inhibits the migration and invasion of HCC cells. The effects of CCT2 knockdown on cancer cell motility were investigated. CCT2 knockdown significantly suppressed the migration and invasion of Huh-7 and HCCLM3 cells, as shown by the gap closure (Fig. 4A and B) and Transwell invasion (Fig. 4C and D) assays. These data demonstrated that CCT2 may be involved in the migration and invasive characteristics of HCC.

Knockdown of CCT2 inhibits the stemness traits of HCC cells. The effect of CCT2 on cancer cell self-renewal was detected by the tumor-sphere formation assay. The number of spheres was lower in the sh-CCT2 compared with the sh-NC group (Fig. 5A and B). Compared with the parental cells in sh-NC group, the spheroid cells in sh-NC group exhibited enhanced proliferative and invasive capacities (Fig. 5C-F). Furthermore, knockdown of CCT2 inhibited these malignant behaviors in both parental and spheroid cells (Fig. 5C-F). Taken together, these findings demonstrated that CCT2 may regulate the stemness traits of HCC cells.

Knockdown of CCT2 inhibits the proliferation and metastasis of HCCLM3 cells in vivo. Subcutaneous xenograft and hematogenous lung metastasis models were used to verify the anticancer effects of CCT2 knockdown *in vivo*. Knockdown of CCT2 in HCCLM3 cells significantly decreased the tumor proliferation rate and final tumor weight in xenograft mice (Fig. 6A and B). Moreover, compared with the sh-NC group, the number of lung metastatic nodules decreased in the sh-CCT2 group (Fig. 6C). In brief, the *in vivo* results confirmed the roles of CCT2 in HCC progression.

Knockdown of CCT2 impairs the activation of STAT3 in HCC cells. Phosphorylation of STAT3, particularly at residue Tyr705, serves as a hallmark of its canonical activation (15). Western blotting showed that knockdown of CCT2 attenuated the phosphorylation levels of STAT3 rather than changing its total protein levels (Fig. 7A and B). In addition, the protein levels of MCL1, MMP2 and SOX2 were downregulated following CCT2 knockdown (Fig. 7A and B). Immunohistochemical staining of subcutaneous tumor tissue also demonstrated that the p-STAT3, MCL1, MMP2 and SOX2 levels were decreased in the sh-CCT2 group (Fig. 7C-F). These results suggested that the STAT3 signaling pathway may be a key downstream pathway regulated by CCT2 in HCC cells.

IL-6 abolishes the effects of CCT2 knockdown in HCC cells. To assess whether the oncogenic effects of CCT2 were dependent on the activation of STAT3, recombinant human IL-6 (50 ng/ml) was used to activate STAT3 signaling in HCC cells. The western blotting results confirmed that IL-6 treatment increased the levels of p-STAT3 in Huh-7 and HCCLM3 cells (Fig. 8A and B). Furthermore, compared with the PBS treatment group, the inhibitory effects of CCT2 knockdown on the proliferation (Fig. 8C and D) and invasion (Fig. 8E and F) of Huh-7 and HCCLM3 cells were significantly abrogated by IL-6 treatment. These results indicated that CCT2 exerts its tumor-promoting effects via STAT3 activation.

Discussion

Despite targeted therapy improving the prognosis of patients with HCC, a notable number of patients experience suboptimal outcomes owing to drug resistance or treatment-associated toxicities (30). Identification of novel molecular targets to improve the outcome of these patients is clinically meaningful.

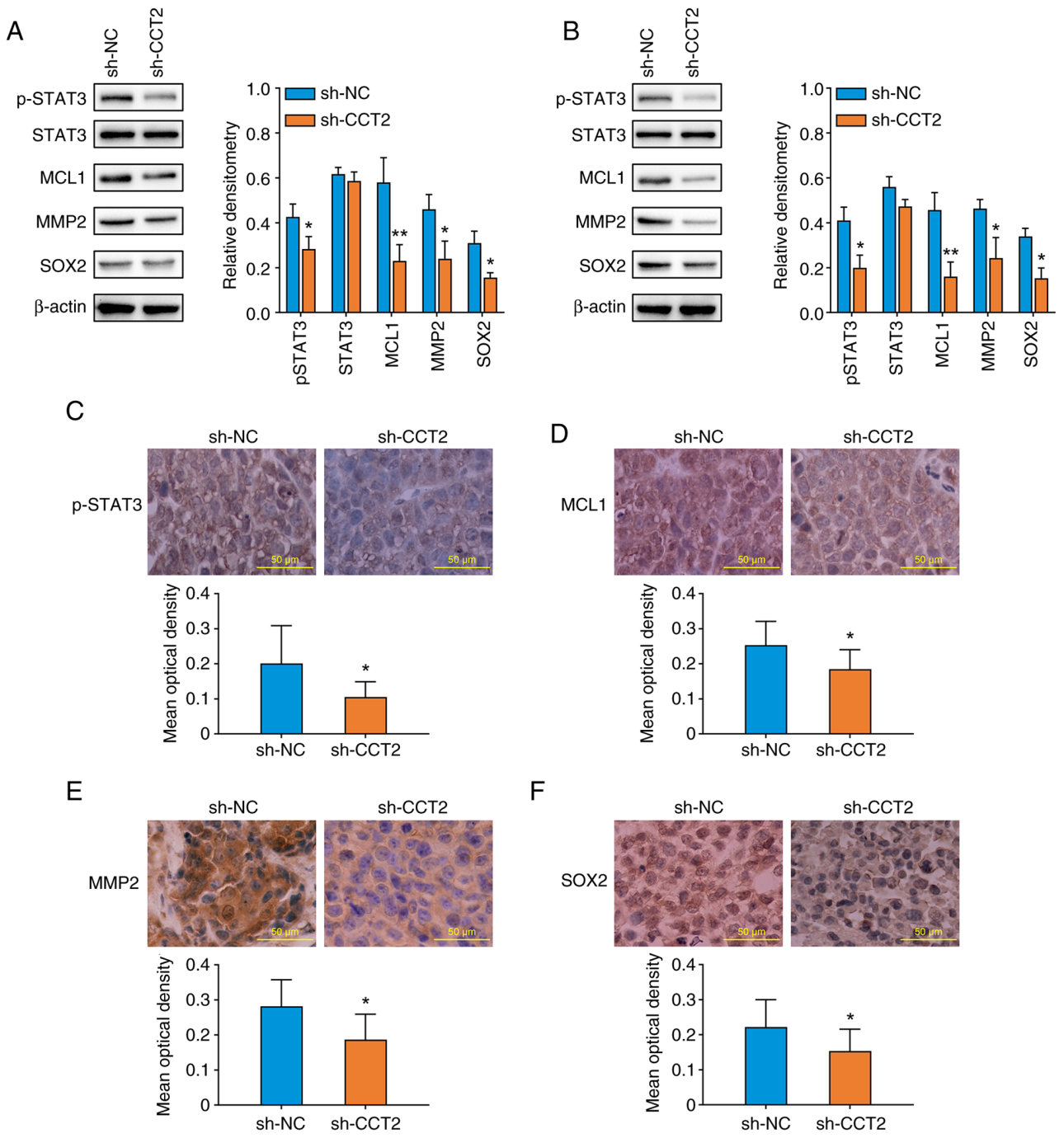

Figure 7. Knockdown of CCT2 inhibits STAT3 signaling activation in hepatocellular carcinoma cells. The protein levels of STAT3, p-STAT3, MCL1, MMP2 and SOX2 in (A) Huh-7 and (B) HCCLM3 cells were measured by western blotting. The protein levels of (C) p-STAT3, (D) MCL1, (E) MMP2 and (F) SOX2 in subcutaneous tumor tissue were detected by immunohistochemical staining. *P<0.05, **P<0.01 vs. sh-NC. CCT2, chaperonin containing TCP1 subunit 2; sh, short hairpin; NC, negative control; p, phosphorylated; MCL1, myeloid cell leukemia sequence 1; SOX2, SRY-box transcription factor 2.

Several studies have investigated the participation of the CCT subunits in oncogenesis mechanisms and found an association between these subunits and hallmarks of malignant cells (31,32). The present study showed that CCT2 promoted cell functions typical of malignancy in HCC.

In the present study, *in silico* analysis revealed that CCT2 expression was typically elevated in HCC tissues and associated with a poorer OS across multiple independent clinical cohorts. In agreement with these findings, CCT2 upregulation is a hallmark of poor prognosis in gallbladder (33), breast (34) and gastric (35) cancer. These results suggest CCT2 may exert key oncogenic roles in HCC progression. In colorectal cancer, CCT2 knockdown inhibits cell proliferation, migration and invasion by interrupting the folding of GLI family zinc finger 1 (36). In the present study, lentiviral-mediated shRNA transduction was used to knockdown the expression of CCT2 in HCC cells. CCT2 knockdown not only attenuated the malignant behaviors, including proliferation, migration and invasion, but also induced the apoptosis of HCC cells. Cancer stem cells promote tumor proliferation and invasion (37,38). The present study found CCT2 knockdown impaired self-renewal as well as the proliferative and invasive properties of spheroid HCC cells. Moreover, in both

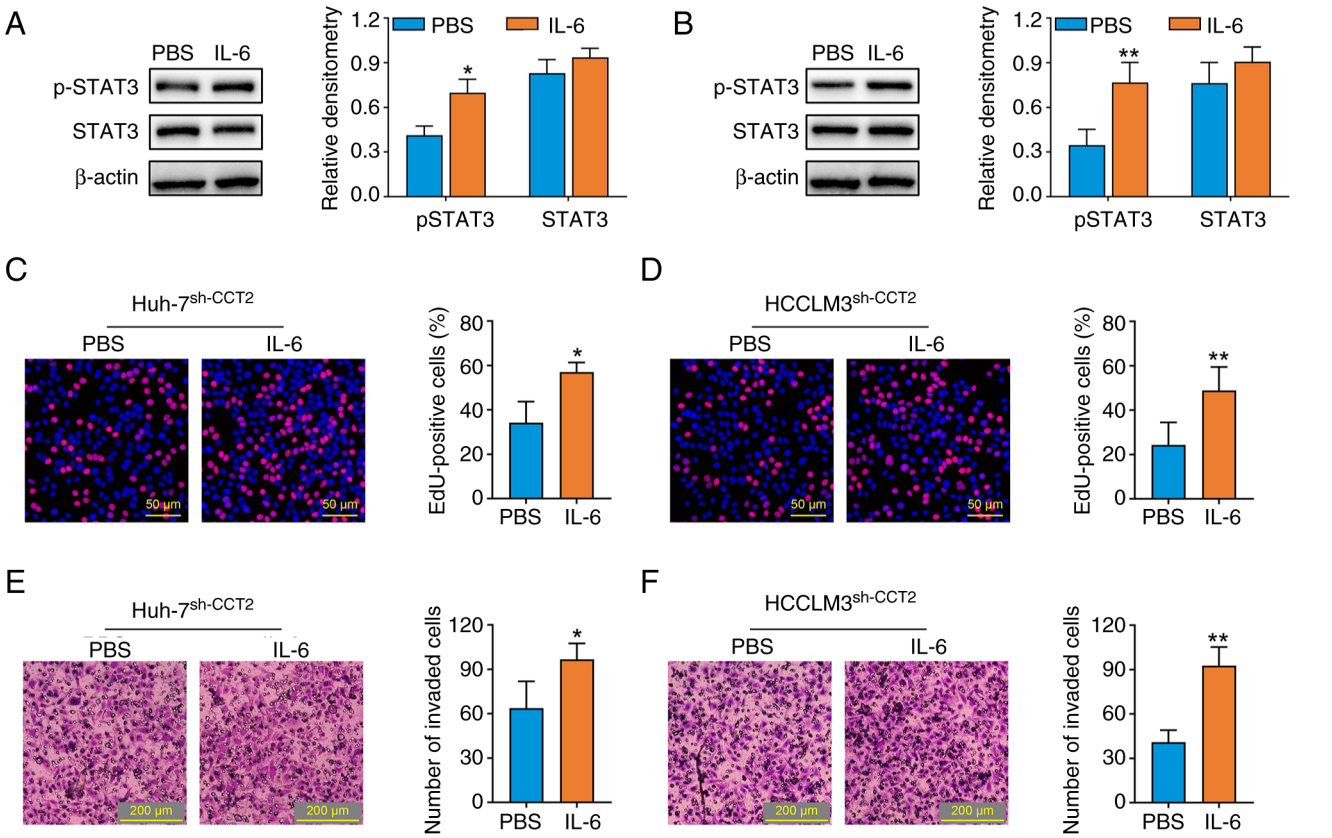

Figure 8. IL-6 abolishes the effects of CCT2 knockdown on the proliferation and invasion of hepatocellular carcinoma cells. The protein levels of STAT3 and p-STAT3 in (A) Huh-7 and (B) HCCLM3 cells were measured by western blotting. The proliferation of (C) Huh-7 and (D) HCCLM3 cells following CCT2 knockdown and IL-6 treatment was detected using EdU incorporation assay. The invasion of (E) Huh-7 and (F) HCCLM3 cells was assessed using Transwell assay. *P<0.05, **P<0.01 vs. PBS. CCT2, chaperonin containing TCP1 subunit 2; sh, short hairpin; p-, phosphorylated.

the subcutaneous xenograft and hematogenous lung metastasis models, CCT2 knockdown inhibited the proliferation and lung metastasis of HCC cells *in vivo*. To the best of our knowledge, the present study is the first to report that CCT2 serves as a driver of HCC proliferation, stemness and invasion.

STAT3 is an oncogene in cancer development. Kasembeli *et al* (39) found that CCT2 knockdown decreases the expression of total STAT3 protein in HS-578T breast cancer cells. However, knockdown of CCT3 sensitizes A549 lung adenocarcinoma cells to cisplatin treatment by inhibiting the phosphorylation of STAT3 (40). Additionally, overexpression of CCT4 partly rescues the inactivation of p-STAT3 induced by anticarin-β in MG-63 osteosarcoma cells (41). The aforementioned reports suggested that the regulation of STAT3 by CCT subunits is mediated by its phosphorylated activation. The present study demonstrated that CCT2 knockdown inactivated the STAT3 signaling pathway in HCC. CCT2 knockdown decreased the levels of p-STAT3, MCL1, MMP2 and SOX2 in HCC cells. As downstream targets of STAT3, MCL1, MMP2 and SOX2 promote HCC progression by driving cell viability, extracellular matrix degradation and self-renewal (14). Exogenous IL-6 treatment rescued the phosphorylation of STAT3 and abrogated the tumor-suppressive effects induced by CCT2 knockdown. Collectively, the present study indicated that CCT2 promotes the malignant behaviors of HCC cells by activating the STAT3 signaling pathway. Notably, CCT2 promotes cancer progression through multiple molecular mechanisms. For example, CCT2 directly binds to KRAS, leading to the increased stability, viability and proliferation of glioblastoma multiforme cells (42). Additionally, epithelial-mesenchymal transition (EMT) causes cancer cells to acquire aggressive phenotypes. CCT2 promotes the EMT process by upregulating the expression of EMT-associated transcription factors, such as zinc finger E-box binding homeobox 1 (43) and Snail/Slug (44). These findings provide a basis to investigate the mechanisms by which CCT2 promotes HCC progression.

The present study had several limitations that should be acknowledged. First, the comprehensive mechanisms by which CCT2 enhances STAT3 phosphorylation remain unclear. Subsequent studies should assess protein-protein interactions to explore how CCT2 activates STAT3 signaling, such as by stabilizing its structure or facilitating its folding. Second, the clinical significance of CCT2 was not evaluated using a prospective patient cohort. A high-quality case-control study should be performed to assess the clinical value of CCT2 in distinguishing healthy controls and HCC.

In conclusion, the present study suggested that CCT2 promoted the malignant behaviors of HCC cells by activating the STAT3 signaling pathway. CCT2 may serve as a promising therapeutic target for patients with HCC.

Acknowledgements

Not applicable.

Funding

The present study was supported by grants from the Beijing Hospitals Authority Youth Programme (grant no. QML20210906) and the Natural Science Basic Research Program of Shaanxi (grant no. 2021JQ-397).

Availability of data and materials

The data generated in this study can be requested from the corresponding author.

Authors' contributions

CL and HQ conceptualized the present study. CL wrote the manuscript. CL, LY and YZ performed experiments. CL, BZ and HQ analyzed the data. All authors have read and approved the final manuscript. CL and HQ confirm the authenticity of all the raw data.

Ethics approval and consent to participate

The animal experiments were approved by the Institutional Animal Care and Use Committee of SPF Biotechnology Co. Ltd. (approval no. AWE2023102504; Beijing, China).

Patient consent for publication

Not applicable.

Competing interests

The authors declare that they have no competing interests.

References

1. Hwang SY, Danpanichkul P, Agopian V, Mehta N, Parikh ND, Abou-Alfa GK, Singal AG and Yang JD: Hepatocellular carcinoma: Updates on epidemiology, surveillance, diagnosis and treatment. Clin Mol Hepatol 31 (Suppl): S228-S254, 2025.
2. Mak LY, Liu K, Chirapongsathorn S, Yew KC, Tamaki N, Rajaram RB, Panlilio MT, Lui R, Lee HW, Lai JC, *et al*: Liver diseases and hepatocellular carcinoma in the Asia-Pacific region: Burden, trends, challenges and future directions. Nat Rev Gastroenterol Hepatol 21: 834-851, 2024.
3. Huang A, Yang XR, Chung WY, Dennison AR and Zhou J: Targeted therapy for hepatocellular carcinoma. Signal Transduct Target Ther 5: 146, 2020.
4. Kim H, Park J and Roh SH: The structural basis of eukaryotic chaperonin TRiC/CCT: Action and folding. Mol Cells 47: 100012, 2024.
5. Gruber R and Horovitz A: Allosteric mechanisms in chaperonin machines. Chem Rev 116: 6588-6606, 2016.
6. Date Y, Matsuura A and Itakura E: Disruption of actin dynamics induces autophagy of the eukaryotic chaperonin TRiC/CCT. Cell Death Discov 8: 37, 2022.
7. Gestaut D, Zhao Y, Park J, Ma B, Leitner A, Collier M, Pintilie G, Roh SH, Chiu W and Frydman J: Structural visualization of the tubulin folding pathway directed by human chaperonin TRiC/CCT. Cell 185: 4770-4787.e20, 2022.
8. Zhu HH, Liu QH, Meng QN, Zhang LJ, Ju SW, Lang JH, Zhu DH, Chen YX, Aishan N, Ouyang XX, *et al*: CCT3/ACTN4/TFRC axis protects hepatocellular carcinoma cells from ferroptosis by inhibiting iron endocytosis. J Exp Clin Canc Res 43: 245, 2024.
9. Li F, Liu CS, Wu P, Ling AS, Pan Q and Li XN: CCT4 suppression inhibits tumor growth in hepatocellular carcinoma by interacting with Cdc20. Chin Med J (Engl) 134: 2721-2729, 2021.
10. Huang XD, Wang XX, Cheng C, Cai J, He S, Wang H, Liu F, Zhu CL, Ding ZM, Huang XT, *et al*: Chaperonin containing TCP1, subunit 8 (CCT8) is upregulated in hepatocellular carcinoma and promotes HCC proliferation. Apmis 122: 1070-1079, 2014.
11. Lv W, Shi L, Pan J and Wang S: Comprehensive prognostic and immunological analysis of CCT2 in pan-cancer. Front Oncol 12: 986990, 2022.
12. Showalter AE, Martini AC, Nierenberg D, Hosang K, Fahmi NA, Gopalan P, Khaled AS, Zhang W and Khaled AR: Investigating Chaperonin-containing TCP-1 subunit 2 as an essential component of the chaperonin complex for tumorigenesis. Sci Rep 10: 798, 2020.
13. Carr AC, Khaled AS, Bassiouni R, Flores O, Nierenberg D, Bhatti H, Vishnubhotla P, Manuel JP, Santra S and Khaled AR: Targeting chaperonin containing TCP1 (CCT) as a molecular therapeutic for small cell lung cancer. Oncotarget 8: 110273-110288, 2017.
14. Hu Y, Dong Z and Liu K: Unraveling the complexity of STAT3 in cancer: Molecular understanding and drug discovery. J Exp Clin Cancer Res 43: 23, 2024.
15. Berkley K, Zalejski J and Sharma A: Targeting STAT3 for cancer therapy: Focusing on Y705, S727, or dual inhibition? Cancers (Basel) 17: 755, 2025.
16. Xu J, Zeng X, Huang J, Ma S, Li K, Yang S, Naz W, Yousaf T, Yuan S, Liu Y, *et al*: Dual-specificity tyrosine-regulated kinase 4 modulates the STAT3-FOS signaling axis to inhibit hepatitis B virus replication via autophagy. Int J Biol Sci 21: 2415-2429, 2025.
17. Tulahong A, Xu X, Zhou T, Ruze R, Yuan Z, Qiao P, Jiang T, Aji T and Shao Y: Empagliflozin alleviates hepatic ischemia-reperfusion injury by inhibiting c-Myc through the JAK1-STAT3 signaling pathway. Int Immunopharmacol 165: 115508, 2025.
18. Nian F, Chen Y, Chen J, Jiang Q, Meng F, Chen Z, Lu X, Shen X and Li Y: Carpaine alleviates NASH-related fibrosis by targeting Nid1 to inhibit IL-6/JAK/STAT3 signaling and macrophage M1 polarization. Int J Biol Macromol 337: 149451, 2025.
19. Hashemi M, Sabouni E, Rahmanian P, Entezari M, Mojtabavi M, Raei B, Zandieh MA, Behroozaghdam M, Mirzaei S, Hushmandi K, *et al*: Deciphering STAT3 signaling potential in hepatocellular carcinoma: Tumorigenesis, treatment resistance, and pharmacological significance. Cell Mol Biol Lett 28: 33, 2023.
20. Chen X, Ma CN, Li YM, Liang YR, Chen T, Han DW, Luo D, Zhang N, Zhao WJ, Wang LJ, *et al*: Trim21-mediated CCT2 ubiquitination suppresses malignant progression and promotes $CD4^{+}$T cell activation in breast cancer. Cell Death Dis 15: 542, 2024.
21. Vallin J, Córdoba-Beldad CM and Grantham J: Sequestration of the transcription factor STAT3 by the molecular chaperone CCT: A potential mechanism for modulation of STAT3 phosphorylation. J Mol Biol 433: 166958, 2021.
22. Cancer Genome Atlas Research Network. Electronic address: wheeler@bcm.edu and Cancer Genome Atlas Research Network: Comprehensive and integrative genomic characterization of hepatocellular carcinoma. Cell 169: 1327-1341.e23, 2017.
23. Fujimoto A, Furuta M, Totoki Y, Tsunoda T, Kato M, Shiraishi Y, Tanaka H, Taniguchi H, Kawakami Y, Ueno M, *et al*: Whole-genome mutational landscape and characterization of noncoding and structural mutations in liver cancer. Nat Genet 48: 500-509, 2016.
24. Gao Q, Zhu H, Dong L, Shi W, Chen R, Song Z, Huang C, Li J, Dong X, Zhou Y, *et al*: Integrated Proteogenomic characterization of HBV-related hepatocellular carcinoma. Cell 179: 561-577, 2019.
25. Jiang Z, Wu Y, Miao Y, Deng K, Yang F, Xu S, Wang Y, You R, Zhang L, Fan Y, *et al*: HCCDB v2.0: Decompose expression variations by Single-cell RNA-seq and spatial Transcriptomics in HCC. Genomics Proteomics Bioinformatics 22: qzae011, 2024.
26. Li C, Cheng X and Jiang Y: Deuterium-depleted water inhibits the malignant progression of colorectal cancer cells by modulating oxidative stress. Oncol Rep 53: 70, 2025.
27. Li C, Miao R, Zhang J, Qu K and Liu C: Long non-coding RNA KCNQ1OT1 mediates the growth of hepatocellular carcinoma by functioning as a competing endogenous RNA of miR-504. Int J Oncol 52: 1603-1612, 2018.
28. Livak KJ and Schmittgen TD: Analysis of relative gene expression data using real-time quantitative PCR and the 2(-Delta Delta C(T)) method. Methods 25: 402-408, 2001.

29. Ranjbar R, Behzadi P and Mammina C: Respiratory tularemia: Francisella tularensis and microarray probe designing. Open Microbiol J 10: 176-182, 2016.
30. Qin Y, Han S, Yu Y, Qi D, Ran M, Yang M, Liu Y, Li Y, Lu L, Liu Y and Li Y: Lenvatinib in hepatocellular carcinoma: Resistance mechanisms and strategies for improved efficacy. Liver Int 44: 1808-1831, 2024.
31. Macario AJL and Conway de Macario E: Chaperonins in cancer: Expression, function, and migration in extracellular vesicles. Semin Cancer Biol 86: 26-35, 2022.
32. Grantham J: The molecular chaperone CCT/TRiC: An essential component of proteostasis and a potential modulator of protein aggregation. Front Genet 11: 172, 2020.
33. Zou Q, Yang ZL, Yuan Y, Li JH, Liang LF, Zeng GX and Chen SL: Clinicopathological features and CCT2 and PDIA2 expression in gallbladder squamous/adenosquamous carcinoma and gallbladder adenocarcinoma. World J Surg Oncol 11: 143, 2013.
34. Liu Q, Qi Y, Kong X, Wang X, Zhang W, Zhai J, Yang Y, Fang Y and Wang J: Molecular and clinical characterization of CCT2 expression and prognosis via Large-scale transcriptome profile of breast cancer. Front Oncol 11: 614497, 2021.
35. Ma X, Qiu SP, Tang X, Song QY, Wang PC, Wang JW, Xia QC, Wang ZJ, Zhao QH and Lu M: TSPAN31 regulates the proliferation, migration, and apoptosis of gastric cancer cells through the METTL1/CCT2 pathway. Transl Oncol 20: 101423, 2022.
36. Park SH, Jeong S, Kim BR, Jeong YA, Kim JL, Na YJ, Jo MJ, Yun HK, Kim DY, Kim BG, *et al*: Activating CCT2 triggers Gli-1 activation during hypoxic condition in colorectal cancer. Oncogene 39: 136-150, 2020.
37. Li YF, Su S, Luo Y, Wei C, He J, Song LD, Han K, Wang J, Gan X and Wang DL: Widespread activation and critical role of EMT and stemness in the neuroendocrine differentiation of prostate cancer (Review). Oncol Rep 54: 109, 2025.
38. Ham A, Cho MH, Won HS, Jo J and Lee KE: β-catenin blockers enhance the effect of CDK4/6 inhibitors on stemness and proliferation suppression in endocrine-resistant breast cancer cells. Oncol Rep 48: 130, 2022.
39. Kasembeli M, Lau WCY, Roh SH, Eckols TK, Frydman J, Chiu W and Tweardy DJ: Modulation of STAT3 folding and function by TRiC/CCT Chaperonin. PLoS Biol 12: e1001844, 2014.
40. Xu DN, Zeng JZ, Sun HM, Pan YL, Yang CC and Lu YD: Chaperonin containing TCP1 subunit 3 (CCT3) promotes cisplatin resistance of lung adenocarcinoma cells through targeting the Janus kinase 2/signal transducers and activators of transcription 3 (JAK2/STAT3) Pathway. Bioengineered 12: 7335-7347, 2021.
41. Wang G, Zhang M, Meng P, Long CB, Luo XD, Yang XW, Wang YF, Zhang ZY, Mwangi J, Kamau PM, *et al*: Anticarin-β shows a promising anti-osteosarcoma effect by specifically inhibiting CCT4 to impair proteostasis. Acta Pharm Sin B 12: 2268-2279, 2022.
42. Zhao FH, Yao Z, Li YQ, Zhao WB, Sun YF, Yang XB, Zhao ZM, Huang B, Wang J, Li XA, *et al*: Targeting the molecular chaperone CCT2 inhibits GBM progression by influencing KRAS stability. Cancer Lett 590: 216844, 2024.
43. Chen JY, Hu Q, Zhou CH and Jin DW: CCT2 prevented β-catenin proteasomal degradation to sustain cancer stem cell traits and promote tumor progression in epithelial ovarian cancer. Mol Biol Rep 51: 54, 2024.
44. Liu WP, Lin RZ, Zhu CM, Chen YXZ, Gao QA and Zhong JJ: CCT2 regulates ZEB1-induced EMT gene transcription to promote the metastasis and tumorigenesis of papillary thyroid carcinoma. Discov Med 36: 1819-1830, 2024.